Uncertainty and Temporal Consistency for Domain-Adaptive Bearing Fault Diagnosis

Chenxuan Huan, Rui Xi*
School of Computer Science and Engineering
UESTC
Chengdu, China
chenxuan980@outlook.com,xirui@uestc.edu.cn

Shilei Zhou
Xi'an Rainbow Intelligent Engineering CO. Ltd.
Xi'an, China
176572446@qq.com

Mengshu Hou,Yalan Ye
School of Computer Science and Engineering
UESTC
Chengdu, China
{mshou,yalanye}@uestc.edu.cn

Yan Linghu
China Construction Silk Road Construction Investment Co., Ltd.
Xi'an, China
326441278@qq.com

***Abstract*—Bearing fault diagnosis is essential for industrial machinery reliability, but domain shifts from varying operational conditions often degrade model performance. While domain adaptation techniques mitigate this issue, challenges like unreliable pseudo-labels and lack of sample evaluation mechanisms remain critical bottlenecks. This paper proposes UTC-DA, a novel approach leveraging uncertainty and temporal consistency for domain-adaptive bearing fault diagnosis. UTC-DAintegrates two key modules: (1) a data augmentation-based pseudo-label voting strategy, enhancing robustness through majority voting on perturbed samples; (2) an uncertainty-aware sample selection mechanism, balancing sample discriminability and diversity by dynamically weighting predictions based on entropy and neighborhood consistency; and filtering high-confidence samples by tracking temporal stability. Experiments on PU and JNU bearing datasets show that UTC-DA outperforms existing state-of-the-art methods in diverse cross-domain tasks, validating UTC-DA's generalization capabilities and practical utility in real-world industrial applications.**

***Index Terms*—Bearing Fault Diagnosis, Domain Adaptation, Pseudo-label Reliability, Uncertainty Estimation, Historical Prediction Consistency.**

I. Introduction

Intelligent fault diagnosis of mechanical equipment, particularly rolling bearings, plays a crucial role in ensuring industrial safety and operational efficiency [1], [2]. Bearing fault diagnosis aims to identify bearing health conditions using sensing signals such as vibration and acoustic emission. In recent years, data-driven diagnostic methods have garnered significant attention. This is particularly true in cross-domain scenarios, where variations in operational conditions induce substantial distribution shifts between source and target data.

Traditional fault diagnosis methods [3] typically rely on large amounts of labeled data and assume consistent data distributions between training and deployment stages, which limits their applicability in real industrial environments. To alleviate this issue, domain adaptation techniques have been introduced to extract transferable features through feature alignment and adversarial learning. Related studies have explored strategies such as feature alignment [4], weight redistribution [5], and pre-training followed by fine-tuning [6] to improve cross-domain diagnostic performance.

However, collecting labeled data from target domains is often impractical in industrial scenarios. Domain generalization and source-free domain adaptation (SFDA) therefore aim to enable model deployment without access to target-domain labels by learning generalized representations across domains [7]. To address issues such as data imbalance [8] and negative transfer [9], SFDA-based strategies including label voting mechanisms [10] have been proposed to improve robustness under cross-domain shifts. However, most-existing SFDA-based methods still lack mechanisms to evaluate the reliability of pseudo-labeled target samples, leading to performance degradation under severe domain shifts.

In this paper, we present UTC-DA, an *U*ncertainty and *T*emporal *C*onsistency for *D*omain-*A*daptive Bearing Fault Diagnosis. The proposed approach focuses on improving the reliability of pseudo labels during target-domain adaptation by progressively refining them through multiple complementary mechanisms. Specifically, an uncertainty-aware learning strategy is designed

* Corresponding Author
This work was supported in part by the National Key R&D Program of China (No. 2023YFB3308602), National Natural Science Foundation of China (No. U2333211), China Construction Technology R&D Project (No. CSCEC-2023-Z-6).

to regulate the relationship between feature representations and pseudo labels, thereby fostering discriminative and stable cluster formation in the presence of noisy target-domain annotations. In addition, a data augmentation-based voting mechanism is incorporated to evaluate label reliability by aggregating predictions from multiple perturbed views, thereby enhancing robustness against complex operating conditions. Furthermore, historical prediction consistency is incorporated to continuously assess pseudo-label stability over training iterations, which helps suppress the influence of unreliable high-confidence samples.

Experiments conducted on the PU [11] and JNU [12] bearing datasets reveal that UTC-DA outperforms state-of-the-art methods across a variety of cross-domain tasks, achieving average accuracies of 99.19% and 97.52%, respectively. These results significantly exceed those of existing methodologies, thereby validating their robust generalization capability and practical applicability in real-world industrial settings.

In summary, the main contributions of this work are as follows:

- We propose an uncertainty-aware source-free domain adaptation framework for bearing fault diagnosis, which explicitly models the reliability of pseudo labels and enables robust cross-domain adaptation without access to source-domain data.
- Within this framework, a high-confidence pseudo-label refinement strategy is developed by jointly considering uncertainty estimation, data augmentation-based voting, neighborhood consistency, and historical prediction consistency, which effectively mitigates the negative impact of unreliable pseudo-labeled samples during target-domain adaptation.
- Thorough evaluations on two public datasets show that our method achieves competitive performance against state-of-the-art methods, demonstrating its effectiveness and superiority.

II. Related Works

A. Unsupervised Domain Adaptation-based Diagnosis

Unsupervised domain adaptation (UDA) aims to achieve accurate predictions on unlabeled target data by leveraging labeled source data while reducing cross-domain distribution discrepancies [13]. Grounded in statistical learning theory [14], UDA methods have been widely applied across various fields. Existing studies can be broadly categorized into metric-based, adversarial-based, and hybrid approaches.

Metric-based methods mitigate domain shift by aligning statistical distributions between domains, with representative techniques including Maximum Mean Discrepancy (MMD) [15] and Correlation Alignment (CORAL) [16]. Adversarial-based approaches employ adversarial learning to automate feature alignment, such as gradient reversal mechanisms used in DANN [17] and separate domain encoders in ADDA [18]. Hybrid methods combine metric learning and adversarial objectives to enhance transferability, including multi-fault networks and attention-enhanced alignment strategies.

B. Source-Free Domain Adaptation-based Diagnosis

Source-free domain adaptation focuses on adapting pre-trained models to unlabeled target domains without access to source data, which is particularly important under data privacy constraints [19]. SHOT established a foundational SFDA framework by integrating pseudo-labeling with information maximization [20]. Subsequent studies extended SFDA to rotating machinery fault diagnosis through information-theoretic optimization and self-training strategies [21].

Recent SFDA research has explored contrastive learning frameworks [22], self-distillation mechanisms [23], and data augmentation techniques such as manifold mixup [24]. Uncertainty-aware methods [25] and clustering-based approaches [26] have also been investigated to improve feature discrimination and pseudo-label reliability under complex operating conditions.

III. Methodology

A. Model Overview

Figure 1 illustrates the overall workflow of the proposed UTC-DA framework, which follows a unified source-free domain adaptation paradigm for bearing fault diagnosis. The framework consists of two stages: supervised model pre-training in the source domain and uncertainty-aware model adaptation in the target domain.

In the pre-training stage, the model is trained in a supervised manner using labeled source domain samples. Specifically, the model is optimized by minimizing the cross-entropy loss $\mathcal{L}_{CE}$ computed over the source domain dataset D_s. The cross-entropy loss $\mathcal{L}_{CE}$ is

$$\mathcal{L}_{CE} = -\mathbb{E}(x_i^s, y_i^s) \in \mathcal{D}_s \sum c = 1^C q_c \log \sigma_c \left(g\left(f(x_i^s)\right)\right) \tag{1}$$

Here, C is the total number of classes, q denotes the one-hot encoded label where $q_c = 1$ for the ground-truth class and 0 otherwise, and $\sigma_c(g(f(x_i^s)))$ is the predicted probability of x_i^s belonging to class c. Minimizing $\mathcal{L}_{CE}$ encourages the model to assign higher probabilities to correct classes, thereby learning discriminative features. The resulting parameters of f and g are transferred to the target domain.

In the target-domain adaptation stage, UTC-DA focuses on progressively improving pseudo-label reliability through several complementary functional modules. First, a multi-view data augmentation and pseudo-label voting module generates diverse target-domain samples via Gaussian noise injection and random scaling, and

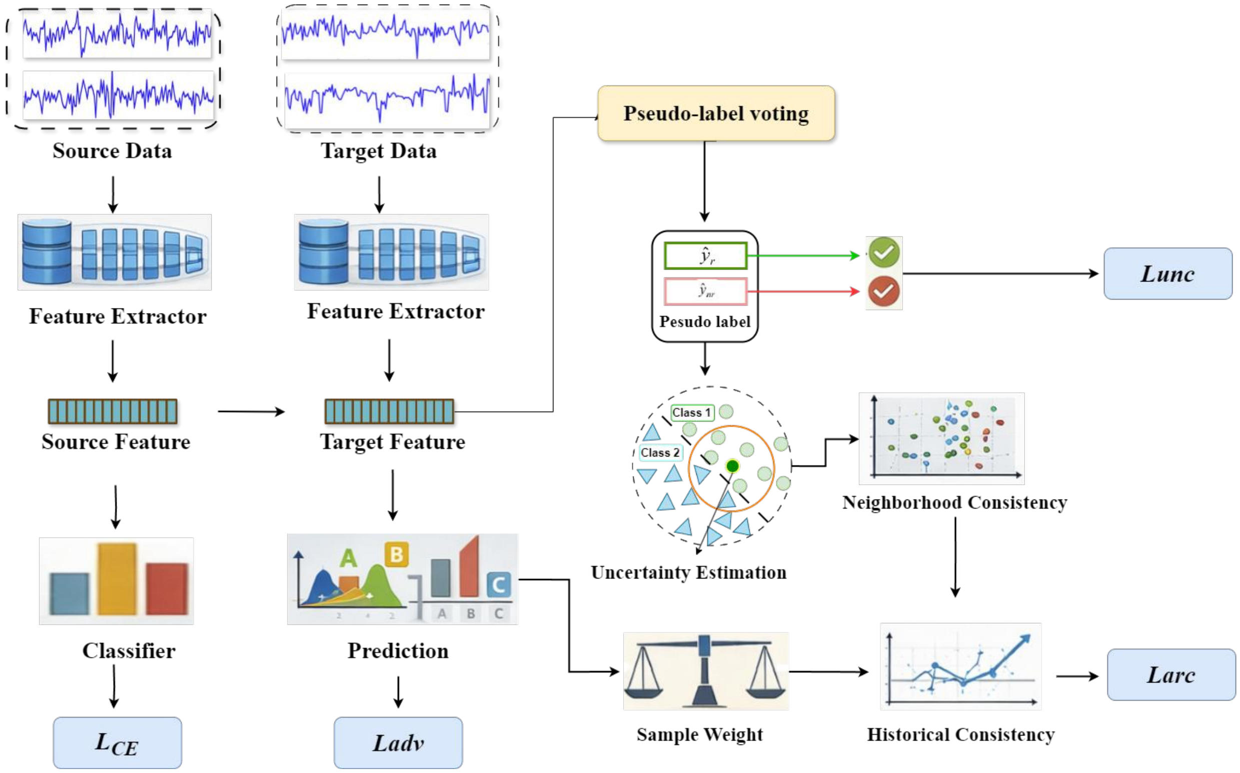

Fig. 1: UTC-DA Framework Overview

assigns initial pseudo labels based on voting consensus. Then, an uncertainty estimation module evaluates pseudo-label reliability by jointly modeling prediction uncertainty and neighborhood consistency in the feature space. In addition, a historical prediction consistency module tracks temporal stability across training iterations to suppress unreliable samples and dynamically adjust their contributions during optimization.

To further alleviate domain shift and enhance discriminative ability, multiple loss functions are collaboratively optimized during adaptation. Specifically, adversarial loss $\mathcal{L}_{adv}$ aligns feature distributions between domains, uncertainty-aware loss $\mathcal{L}_{unc}$ suppresses unreliable pseudo labels while preserving feature diversity, and feature discrimination loss $\mathcal{L}_{arc}$ enhances class separability by enforcing clear decision boundaries in the target domain.

B. Pseudo-Label Reliability Enhancement Modules

1) Robust Pseudo-Label Generation: Following the overall framework, robust pseudo-label generation serves as the first step to initialize supervision signals for target-domain adaptation. Multiple augmented views are generated for each target sample, and prediction consensus across views is exploited to reduce the influence of domain shift.

Majority voting is adopted to aggregate predictions from augmented samples. The final pseudo label is determined by:

$$\hat{y}_j = \arg\max_c \sum_{k=1}^{K} \mathbb{I}(\arg\max p_j^{(k)} = c) \tag{2}$$

where K denotes the number of augmentations.

2) Uncertainty-Aware Sample Selection Mechanism: Building upon the generated pseudo labels, an uncertainty-aware weighting mechanism is introduced to evaluate their reliability and adjust sample contributions during optimization. This module jointly considers prediction confidence and neighborhood consistency to quantify pseudo-label uncertainty.

Based on the estimated uncertainty u_j, each target sample is assigned a weight $\omega_j = \exp(-\lambda u_j)$, and the uncertainty-aware loss is formulated as:

$$\mathcal{L}_{unc} = \sum_{j=1}^{N_t} \omega_j \left[\lambda_1 \mathcal{L}_{CE}(p_j^t, y_j^t) + \lambda_2 \mathcal{L}_{div}(p_j^t)\right] \tag{3}$$

where λ, λ_1, and λ_2 are weighting coefficients.

Although uncertainty-aware weighting improves pseudo-label utilization, temporal instability may still exist. To further refine sample reliability, a hard sample filtering mechanism based on historical prediction consistency is introduced as a complementary component of the framework.

Prediction stability is quantified by measuring the divergence between consecutive predictions:

$$\text{Cons}_j^{(t)} = \frac{1}{C}\sum_{c=1}^{C}\left|p_{jc}^{(t)} - p_{jc}^{(t-1)}\right| \tag{4}$$

The corresponding sample weight is dynamically adjusted as:

$$w_j^{(t)} = \frac{1}{1+\beta\cdot\text{Cons}_j^{(t)}} \tag{5}$$

where β controls the influence of temporal consistency.

C. Optimization Strategy

1) Domain Alignment Loss: To address the challenge of domain shift in unsupervised domain adaptation, this work integrates an adversarial domain alignment loss. It employs an adversarial training strategy to learn domain-invariant feature representations. Let $\mathcal{F}$ denote the feature extractor and $\mathcal{D}$ the domain classifier. The adversarial objective is formulated as:

$$\mathcal{L}_{\text{adv}} = \mathbb{E}_{z\sim\mathcal{Z}_s}\left[\log(1-\mathcal{D}(z))\right] + \mathbb{E}_{z\sim\mathcal{Z}_t}\left[\log(\mathcal{D}(z))\right] \tag{6}$$

where $\mathcal{Z}_s$ and $\mathcal{Z}_t$ represent the source and target domain feature distributions, respectively. This formulation promotes feature distribution alignment by optimizing $\mathcal{F}$ to generate features that confuse the domain discriminator $\mathcal{D}$.

2) Feature Discrimination Enhancement Loss: Although domain alignment reduces cross-domain discrepancies, it may weaken class discrimination in the target domain. To compensate for this effect, a feature discrimination enhancement loss is incorporated to explicitly improve class separability.

Specifically, the ArcFace loss introduces an angular margin in the feature space, enlarging inter-class distances while compacting intra-class variations. This property is particularly beneficial under severe domain shifts, where decision boundaries are prone to ambiguity.

The ArcFace loss is defined as:

$$\mathcal{L}_{arc} = -\frac{1}{N_t}\sum_{j=1}^{N_t}\log\left(\frac{e^{s\cos(\theta_{y_j^t}+m)}}{e^{s\cos(\theta_{y_j^t}+m)} + \sum_{c\neq y_j^t} e^{s\cos\theta_c}}\right) \tag{7}$$

where s denotes the feature scaling factor and m controls the angular margin.

3) Total Loss: The comprehensive optimization objective function [27] with uncertainty estimation is formulated as:

$$\mathcal{L}_{\text{total}} = \mathcal{L}_{\text{CE}} + \alpha\mathcal{L}_{\text{unc}} + \mu\mathcal{L}_{\text{adv}} + \zeta\mathcal{L}_{\text{arc}} \tag{8}$$

Here, $\mathcal{L}_{\text{CE}}$ maintains source-domain discriminability, $\mathcal{L}_{\text{unc}}$ improves pseudo-label reliability, $\mathcal{L}_{\text{adv}}$ aligns feature distributions across domains, and $\mathcal{L}_{\text{arc}}$ enhances class separability. The hyperparameters α, μ, and ζ control the contribution of each loss.

IV. Experiments Setup

This section provides a comprehensive evaluation of the proposed passive domain adaptive method based on uncertainty estimation using two publicly available datasets: the JNU dataset and the PU dataset. The experiments aim to demonstrate the advantages of the proposed method over existing approaches in fault diagnosis tasks and analyze its performance under different combinations of loss functions.

A. Datasets

University of Paderborn (PU) Dataset: The PU dataset includes one healthy bearing (K001) and seven faulty bearings (KA04, KA15, KA22, KA30, KI14, KI17, KI21), covering outer-ring and inner-ring faults. It consists of six healthy samples, 12 artificially damaged samples, and 14 naturally worn samples under accelerated loading. Vibration signals were sampled at 64 kHz, with 20 measurements per condition, and truncated to 2048 points. The dataset was divided into three domains: A1 (1500 r/min, 0.1 Nm, 1000 N), A2 (1500 r/min, 0.7 Nm, 400 N), and A3 (1500 r/min, 0.7 Nm, 1000 N).

Jiangnan University (JNU) Dataset: The JNU dataset contains four bearing conditions: healthy (NO), inner-ring (IR), ball (B), and outer-ring (OR) faults, generated via precision-machined micro-indentations. Each signal was truncated to 2048 points, with 2000 samples per category. Based on rotational speed, the dataset was divided into three domains: B1 (600 r/min), B2 (800 r/min), and B3 (1000 r/min).

TABLE I: Details of Network Architecture.

Stage	**Layer Composition**	**Output Shape**
Input	Raw vibration signal	[B, 1, 2048]
Conv Stage 1	Conv + BN + ReLU + MaxPool	[B, 16, 1024]
Conv Stage 2	Conv + BN + ReLU + MaxPool	[B, 32, 512]
Conv Stage 3	Conv + BN + ReLU + MaxPool	[B, 64, 256]
Conv Stage 4	Conv + BN + ReLU + Global AvgPool	[B, 128, 1]
Feature Embedding	Flatten → FC → ReLU → Dropout	[B, 64]
Classifier	FC → Softmax	[B, C]

B. Baselines

The comparative study includes representative transfer learning and domain adaptation methods, summarized as follows.

Statistical Metric-Based Methods: These methods reduce domain discrepancy by aligning statistical distributions. Joint Adaptive Networks (JAN) [28] minimize joint maximum mean discrepancy across layers, while Correlation Alignment (CORAL) [29] aligns second-order statistics between domains.

Adversarial-Based Domain Adaptation Methods: Adversarial training is adopted to learn domain-invariant features. Domain Adversarial Neural Networks

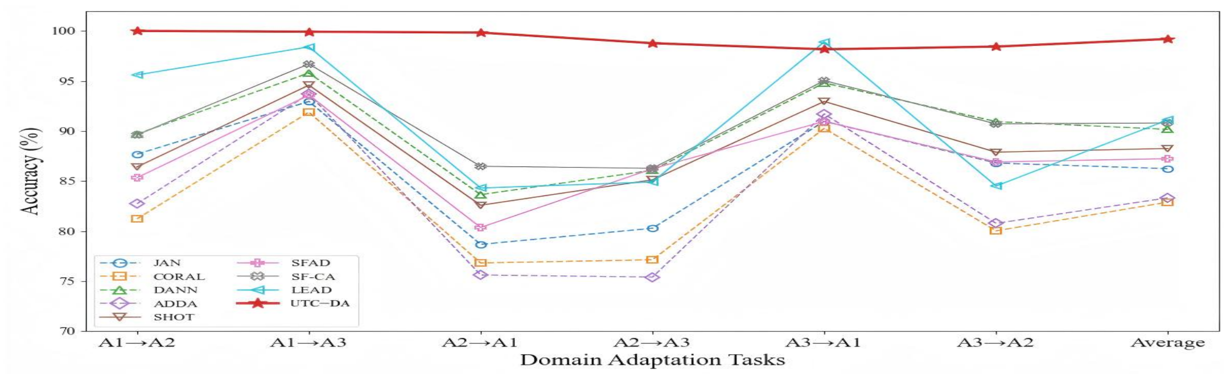

Fig. 2: Performance comparison of different domain adaptation methods on PU datasets

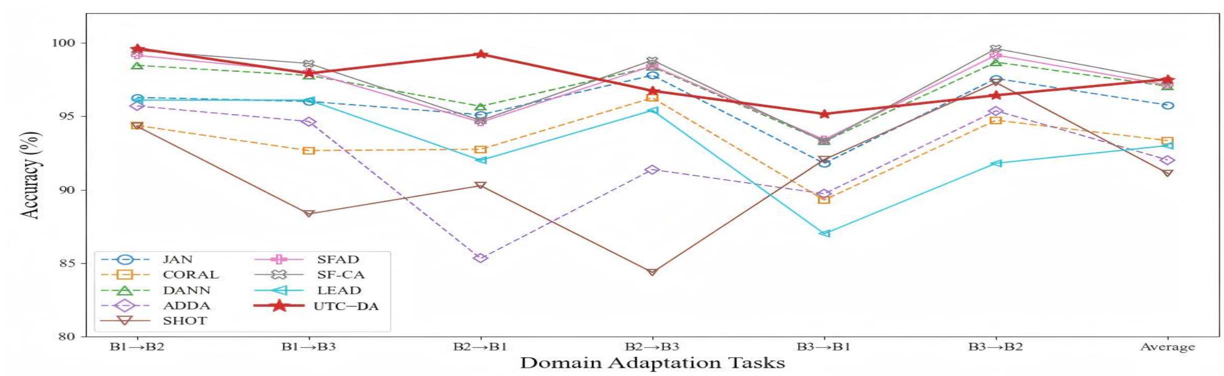

Fig. 3: Performance comparison of different domain adaptation methods on JNU datasets

(DANN) [30] employ a domain discriminator with gradient reversal, whereas Adversarial Discriminative Domain Adaptation (ADDA) [31] performs step-wise adversarial learning to map target features into the source space. Label-Embedded Adversarial Domain Adaptation (LEAD) [32] further enhances adversarial alignment by embedding category-related information into the domain discrimination process, thereby alleviating class confusion during cross-domain adaptation.

Source-Free Domain Adaptation Methods: These approaches adapt models without accessing source data. SHOT [33] combines entropy minimization and self-training with pseudo-labels, while SFAD [21] replaces entropy regularization with kernel norm regularization for fault diagnosis. SF-CA [34] enhances pseudo-label reliability via clustering hypotheses and R-drop with conditional autoencoders.

C. Implemetation Details

Experimental Setup: All methods are trained using the same raw vibration signals to ensure fair comparison. Identical training hyperparameters are adopted across all datasets. The batch size is set to 64, and models are trained for 100 iterations. A learning rate of 0.0001 is used during target adaptation to alleviate overfitting, with the Adam optimizer and a weight decay of 0.0001.

Network Architecture: The proposed framework adopts a lightweight one-dimensional CNN as the feature backbone to extract discriminative representations from raw vibration signals. The backbone network follows a standard architecture consisting of a feature extraction module and a classification module.

The feature extraction module is composed of several stacked convolutional stages, each including a one-dimensional convolution layer, batch normalization, ReLU activation, and a downsampling operation. Through progressively increasing channel dimensions and reducing temporal resolution, the backbone captures hierarchical features that characterize bearing fault patterns at different scales.

The classification module consists of a fully connected layer followed by nonlinear activation and Dropout regularization, producing compact feature embeddings for subsequent prediction. This backbone network serves as a unified feature extractor for the proposed framework, upon which the pseudo-label voting module (M1) and the uncertainty-aware optimization module (M2) are applied during target-domain adaptation.

V. Results

A. Comparison with SOTA

The proposed UTC-DA method was evaluated on the PU and JNU datasets, with results shown in Fig. 2 and Fig. 3. In Fig. 2, the red star-marked curve denotes UTC-DA . Solid lines indicate source-free domain adaptation methods, while dashed lines represent traditional UDA methods. "A1→A2" denotes adaptation from source domain A1 to target domain A2.

As a source-free method, UTC-DA does not require access to source domain data. By incorporating uncertainty estimation into pseudo-label selection, unreliable target samples are effectively filtered during adaptation.

On the PU dataset, UTC-DA achieves the highest average accuracy of 99.19%, outperforming all baseline methods across different transfer tasks. On the JNU dataset, UTC-DA also obtains the best average accuracy of 97.52%, indicating stable performance under varying operating conditions.

Among the compared methods, JAN, CORAL, DANN, and ADDA rely on source-domain data for distribution alignment, while SHOT, SFAD, SF-CA, and LEAD operate in source-free settings. Compared with these approaches, UTC-DA shows more consistent performance across all adaptation directions.

Overall, the superior **average accuracy on both datasets** demonstrates that UTC-DA exhibits strong generalization capability in source-free cross-domain bearing fault diagnosis.

To gain a deeper and more intuitive understanding of the proposed UTC-DA, t-distributed stochastic neighbor embedding (t-SNE) was employed to visualize and analyze the output features from the feature extraction module. Task A1→A2, A1→A3, A2→A1, A2→A3, A3→A1, A3→A2 applied to the PU dataset; B1→B2, B1→B3, B2→B1, B2→B3, B3→B1, B3→B2 applied to the JNU dataset. Fig. 4 and Fig. 5 display feature representations extracted from the final layer of the feature encoder, with different colors representing distinct categories. The visualization for the PU dataset encompasses one healthy state and seven fault states, totaling eight distinct bearing conditions; the JNU dataset displays one healthy state and three fault states, totaling four bearing conditions. The results demonstrate that the features learned by UTC-DA exhibit distinct intra-class clustering and inter-class separation within both the source domain and the target domain.

B. Ablation Studies

Our method incorporates two key components to improve target-domain adaptation: M1 denotes the pseudo-label voting strategy based on data augmentation, and M2 denotes the uncertainty-aware optimization mechanism that integrates prediction uncertainty and historical consistency.

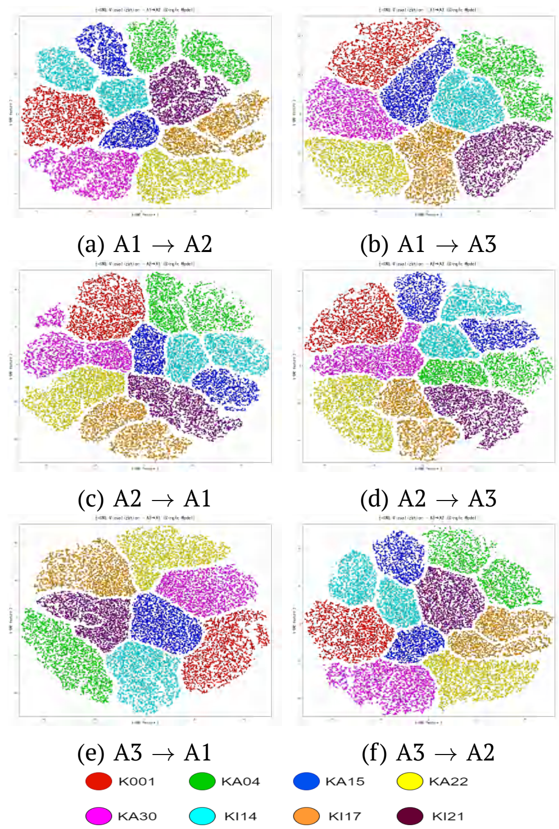

Fig. 4: t-SNE on PU datasets

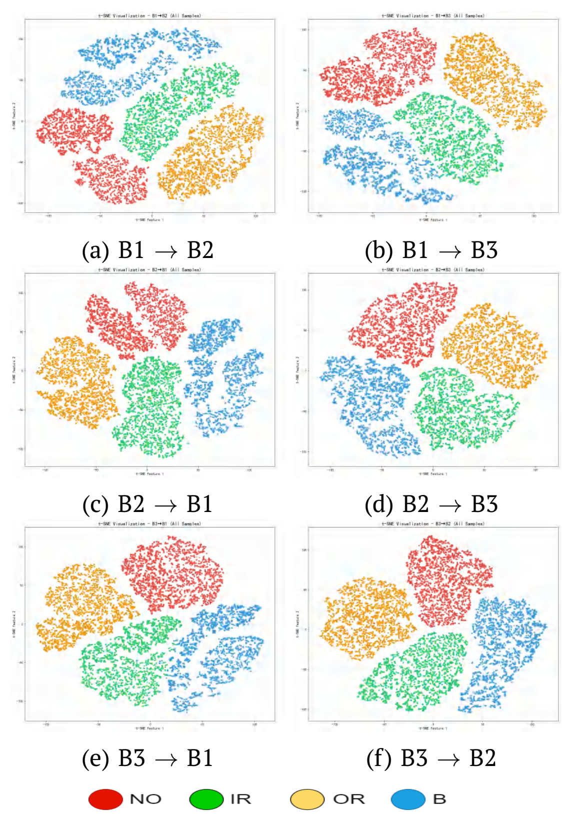

Fig. 5: t-SNE on JNU datasets.

TABLE II: Ablation study on JNU dataset

Methods	B1 → B2	B1 → B3	B2 → B1	B2 → B3	B3 → B1	B3 → B2	Average
Baseline	96.51	95.84	92.38	92.12	90.1	93.81	93.46
Baseline + M1	96.28	97.93	95.13	96.9	96.24	97.5	96.67
Baseline + M1 + M2	99.62	97.92	99.23	96.73	95.16	96.43	97.52

TABLE III: Ablation study on PU dataset

Methods	A1 → A2	A1 → A3	A2 → A1	A2 → A3	A3 → A1	A3 → A2	Average
Baseline	96.51	95.84	96.38	93.12	97.1	96.81	96.96
Baseline + M1	97.28	98.93	98.13	98.9	99.24	98.89	98.56
Baseline + M1 + M2	100	99.92	99.83	98.77	98.16	98.43	99.19

Ablation experiments were conducted on the JNU and PU datasets to evaluate the contribution of each component. The baseline corresponds to the label-reliability-based passive domain adaptation method. On this basis, M1 is introduced to enhance pseudo-label reliability through multi-view majority voting. M2 is further applied to suppress unreliable and high-confidence misclassified samples during optimization.

As shown in Tables II and III, incorporating M1 leads to consistent performance improvements across all cross-domain transfer tasks, indicating that data-augmentation-based voting effectively stabilizes pseudo-label generation. The addition of M2 yields further accuracy gains, demonstrating that uncertainty-guided sample weighting and temporal prediction stability are critical for robust domain adaptation under severe distribution shifts.

C. Hyperparamater Tuning

To assess the model's robustness, we conducted a systematic sensitivity analysis on the uncertainty decay coefficient λ and the historical consistency coefficient β.

When testing the uncertainty decay coefficient, we fixed β = 1.5 and adjusted λ between 0.3 and 1.7 with a step size of 0.2. As shown in Figure, diagnostic accuracy initially increases then decreases as λ rises. When λ is too small, the model struggles to effectively suppress noise from high-uncertainty samples. When λ is too large, excessive attenuation of valid sample information degrades performance. Near λ = 0.8, the model achieves optimal robustness balance.

Subsequently, while examining the historical consistency coefficient, λ was fixed at 0.8, and β was varied from 1.1 to 2.5 in increments of 0.2. As shown in Figure, diagnostic accuracy remains relatively insensitive to β changes, maintaining high levels within the range [1.3, 2.1]. This indicates that model performance primarily depends on the uncertainty assessment controlled by λ, while its dependence on the historical prediction consistency controlled by β is relatively weak, demonstrating the model's excellent stability.

In summary, parameter λ is key to regulating the model's robustness against noisy samples, while parameter β provides a stable and effective auxiliary regularization term for the model.

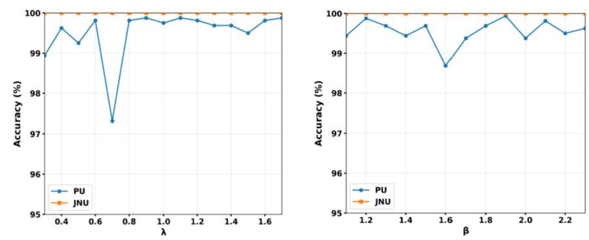

(a) Hyperparameter λ for PU and JNU datasets (b) Parameter β for PU and JNU

Fig. 6: Hyperharameters for PU and JNU datasets

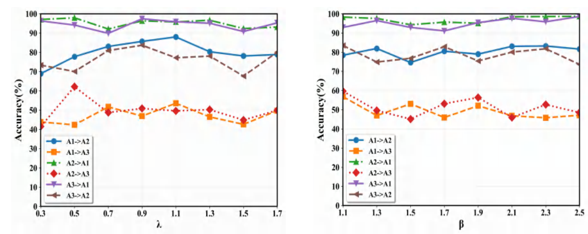

(a) Hyperparameter λ for PU datasets (b) Hyperparameter β for PU datasets

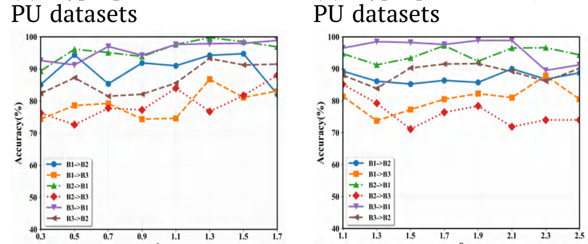

(c) Hyperparameter λ for JNU datasets (d) Hyperparameter β for JNU datasets

Fig. 7: Hyperparameters for PU and JNU

VI. Conclusion

To address the degradation in model performance caused by cumulative pseudo-label noise in source-domain-free adaptation, the proposed UTC-DA method systematically enhances pseudo-label quality and training robustness by integrating uncertainty estimation, data augmentation voting, and historical consistency tracking. Experiments demonstrate optimal performance across multiple cross-domain diagnostic tasks. Feature visualization results reveal clearer class separation, validating the method's effectiveness in learning discriminative domain-invariant features and providing a more reliable solution for unsupervised fault diagnosis. Future work will target more complex open scenarios.

References

[1] Z. Zhu, Y. Lei, G. Qi, Y. Chai, N. Mazur, Y. An, and X. Huang, "A review of the application of deep learning in intelligent fault diagnosis of rotating machinery," *Measurement*, vol. 206, p. 112346, 2023.

[2] M. Xia, H. Shao, D. Williams, S. Lu, L. Shu, and C. W. de Silva, "Intelligent fault diagnosis of machinery using digital twin-assisted deep transfer learning," *Reliability Engineering & System Safety*, vol. 215, p. 107938, 2021.

[3] A. Abid, M. T. Khan, and J. Iqbal, "A review on fault detection and diagnosis techniques: basics and beyond," *Artificial Intelligence Review*, vol. 54, no. 5, pp. 3639–3664, 2021.

[4] S. Liu, H. Jiang, Y. Wang, K. Zhu, and C. Liu, "A deep feature alignment adaptation network for rolling bearing intelligent fault diagnosis," *Advanced engineering informatics*, vol. 52, p. 101598, 2022.

[5] P. Ding, H. Dong, Z. Fei, and X.-M. Sun, "A novel feature separation weight rectified network for mechanical fault diagnosis under partial domain adaptation," *IEEE Transactions on Industrial Informatics*, 2024.

[6] J. Chen, Z. Yan, C. Lin, B. Yao, and H. Ge, "Aero-engine high speed bearing fault diagnosis for data imbalance: A sample enhanced diagnostic method based on pre-training wgan-gp," *Measurement*, vol. 213, p. 112709, 2023.

[7] J. Tian, Y. Jiang, J. Zhang, H. Luo, and S. Yin, "A novel data augmentation approach to fault diagnosis with class-imbalance problem," *Reliability Engineering & System Safety*, vol. 243, p. 109832, 2024.

[8] Z. Ren, T. Lin, K. Feng, Y. Zhu, Z. Liu, and K. Yan, "A systematic review on imbalanced learning methods in intelligent fault diagnosis," *IEEE Transactions on Instrumentation and Measurement*, vol. 72, pp. 1–35, 2023.

[9] Z. Wang, M. Ragab, W. Yang, M. Wu, S. J. Pan, J. Zhang, and Z. Chen, "Overcoming negative transfer by online selection: Distant domain adaptation for fault diagnosis," *IEEE Transactions on Instrumentation and Measurement*, 2024.

[10] V. Shandhoosh, G. Chakrapani, V. Sugumaran, S. M. Ramteke, M. Marian *et al.*, "Intelligent fault diagnosis for tribo-mechanical systems by machine learning: Multi-feature extraction and ensemble voting methods," *Knowledge-Based Systems*, vol. 305, p. 112694, 2024.

[11] K. Li, X. Ping, H. Wang, P. Chen, and Y. Cao, "Sequential fuzzy diagnosis method for motor roller bearing in variable operating conditions based on vibration analysis," *Sensors*, vol. 13, no. 6, pp. 8013–8041, 2013. [Online]. Available: https://www.mdpi.com/1424-8220/13/6/8013

[12] C. Lessmeier, J. K. Kimotho, D. Zimmer, and W. Sextro, "Condition monitoring of bearing damage in electromechanical drive systems by using motor current signals of electric motors: A benchmark data set for data-driven classification," in *PHM society European conference*, vol. 3, no. 1, 2016.

[13] Z. Du, J. Li, H. Su, L. Zhu, and K. Lu, "Cross-domain gradient discrepancy minimization for unsupervised domain adaptation," in *Proceedings of the IEEE/CVF conference on computer vision and pattern recognition*, 2021, pp. 3937–3946.

[14] J. Fan, H. Zhu, X. Jiang, L. Meng, C. Chen, C. Fu, H. Yu, C. Dai, and W. Chen, "Unsupervised domain adaptation by statistics alignment for deep sleep staging networks," *IEEE Transactions on Neural Systems and Rehabilitation Engineering*, vol. 30, pp. 205–216, 2022.

[15] Q. Qian, Y. Wang, T. Zhang, and Y. Qin, "Maximum mean square discrepancy: a new discrepancy representation metric for mechanical fault transfer diagnosis," *Knowledge-Based Systems*, vol. 276, p. 110748, 2023.

[16] Z. Wang, J. Xuan, and T. Shi, "Domain reinforcement feature adaptation methodology with correlation alignment for compound fault diagnosis of rolling bearing," *Expert Systems with Applications*, vol. 262, p. 125594, 2025.

[17] Z. Zhang, M. Shao, C. Ma, Z. Lv, and J. Zhou, "An enhanced domain-adversarial neural networks for intelligent cross-domain fault diagnosis of rotating machinery," *Nonlinear Dynamics*, vol. 108, no. 3, pp. 2385–2404, 2022.

[18] Y. Gao, B. Baucom, K. Rose, K. Gordon, H. Wang, and J. A. Stankovic, "E-adda: Unsupervised adversarial domain adaptation enhanced by a new mahalanobis distance loss for smart computing," in *2023 IEEE International Conference on Smart Computing (SMARTCOMP)*. IEEE, 2023, pp. 172–179.

[19] Q. Li, B. Tang, L. Deng, and P. Zhu, "Source-free domain adaptation framework for fault diagnosis of rotation machinery under data privacy," *Reliability Engineering & System Safety*, vol. 238, p. 109468, 2023.

[20] J. Wu, G. Wang, R. Gu, T. Lu, Y. Chen, W. Zhu, T. Vercauteren, S. Ourselin, and S. Zhang, "Upl-sfda: Uncertainty-aware pseudo label guided source-free domain adaptation for medical image segmentation," *IEEE transactions on medical imaging*, vol. 42, no. 12, pp. 3932–3943, 2023.

[21] J. Jiao, H. Li, T. Zhang, and J. Lin, "Source-free adaptation diagnosis for rotating machinery," *IEEE Transactions on Industrial Informatics*, vol. 19, no. 9, pp. 9586–9595, 2022.

[22] N. Saunshi, J. Ash, S. Goel, D. Misra, C. Zhang, S. Arora, S. Kakade, and A. Krishnamurthy, "Understanding contrastive learning requires incorporating inductive biases," in *International Conference on Machine Learning*. PMLR, 2022, pp. 19 250–19 286.

[23] J. Jiao, T. Zhang, H. Li, H. Liu, and J. Lin, "Source-free blackbox adaptation for machine fault diagnosis," *IEEE Transactions on Industrial Informatics*, 2025.

[24] I. Kaufman and O. Azencot, "First-order manifold data augmentation for regression learning," *arXiv preprint arXiv:2406.10914*, 2024.

[25] Y. Qin, X. Wang, A. Beutel, and E. Chi, "Improving calibration through the relationship with adversarial robustness," *Advances in Neural Information Processing Systems*, vol. 34, pp. 14 358–14 369, 2021.

[26] P. Wu and J. Liu, "Learning causal temporal relation and feature discrimination for anomaly detection," *IEEE Transactions on Image Processing*, vol. 30, pp. 3513–3527, 2021.

[27] W. Wu, Z. Hao, Z. Wei, X.-Y. Jing, Q. Zhang, and S. Wu, "Both reliable and unreliable predictions matter: Domain adaptation for bearing fault diagnosis without source data," *Neurocomputing*, p. 131661, 2025.

[28] M. Long, H. Zhu, J. Wang, and M. I. Jordan, "Deep transfer learning with joint adaptation networks," in *International conference on machine learning*. PMLR, 2017, pp. 2208–2217.

[29] B. Sun and K. Saenko, "Deep coral: Correlation alignment for deep domain adaptation," in *European conference on computer vision*. Springer, 2016, pp. 443–450.

[30] Y. Ganin, E. Ustinova, H. Ajakan, P. Germain, H. Larochelle, F. Laviolette, M. March, and V. Lempitsky, "Domain-adversarial training of neural networks," *Journal of machine learning research*, vol. 17, no. 59, pp. 1–35, 2016.

[31] E. Tzeng, J. Hoffman, K. Saenko, and T. Darrell, "Adversarial discriminative domain adaptation," in *Proceedings of the IEEE conference on computer vision and pattern recognition*, 2017, pp. 7167–7176.

[32] Y. Chen, J. Shi, C. Shen, H. Yang, Z. Hua, W. Huang, and Z. Zhu, "Time-frequency aware feature disentanglement learning for intelligent bearing fault diagnosis under variable speed conditions," *Expert Systems with Applications*, p. 130664, 2025.

[33] J. Liang, D. Hu, and J. Feng, "Do we really need to access the source data? source hypothesis transfer for unsupervised domain adaptation," in *International conference on machine learning*. PMLR, 2020, pp. 6028–6039.

[34] M. Zhu, X. Zeng, J. Liu, C. Yang, and K. Zhou, "Source-free cluster adaptation for privacy-preserving machinery fault diagnosis," *IEEE Transactions on Instrumentation and Measurement*, vol. 72, pp. 1–10, 2023.